Microwave Dielectric Properties of Low-Temperature Sinterable α-MoO_3

Jobin Varghese, Tuomo Siponkoski, Mikko Nelo, Mailadil Thomas Sebastian, and Heli Jantunen

Microelectronics Research Unit, Faculty of Information Technology and Electrical Engineering, P- O. BOX 4500, University of Oulu, 90014, Finland.

Abstract

The α-MoO_3 ceramics were prepared by uniaxial pressing and sintering of MoO_3 powder at 650 ^oC and their structure, microstructure, densification and sintering and microwave dielectric properties were investigated. The sintering temperature of α-MoO_3 was optimized based on the best densification and microwave dielectric properties. After sintering at 650 ^oC the relative permittivity was found to be 6.6 and the quality factor was 41,000 GHz at 11.3 GHz. The full-width half-maximum of the A_{1g} Raman mode of bulk α-MoO_3 at different sintering temperatures correlated well with the Qf values. Moreover, the sintered samples showed a temperature coefficient of the resonant frequency of -25 ppm/^oC in the temperature range from -40 to 85 ^oC and they exhibited a very low coefficient of thermal expansion of ±4 ppm/^oC. These microwave dielectric properties of α-MoO_3 will be of great benefit in future MoO_3 based materials and their applications.

Keywords: Microwave Ceramics; Sintering; Raman Spectroscopy; X-ray photoelectron spectroscopy and Scanning electron microscopy

Introduction

Molybdenum oxide (MoO_3), because of its exceptional properties, has been the subject of much revived interest as a promising candidate for a broad range of applications such as catalysis [1,2], batteries [3, 4], supercapacitors [5], photo and electrochromic devices [6, 7], gas sensors [8], memory devices [9], organic light emitting diodes (OLEDs) [10], Dielectric/insulation applications [11], oxide solar cells [12] , etc. MoO_3 has four polymorph modifications, which include α-MoO_3 (orthorhombic),

β- MoO_3 (monoclinic), high-pressure MoO_3-II and h-MoO_3 (hexagonal). Among these, the α-MoO_3 is a stable polymorph with a bilayer of distorted octahedra having excellent physical properties [13]. It has also been studied in the form of thin films, nanobelts, and nanorods[14-17].

The fast-growing wireless communication networks require ultra-low sintering temperature materials with excellent dielectric properties in the microwave frequency range. In addition, these materials further reduce the cost of production of a range of communication and consumer electronic products. The recent review of Ultra-Low Temperature Co-fired Ceramic (ULTCC) materials with sintering temperatures below 700 ^oC by Sebastian *et. al.* [18], shows that most of the reported compositions are based on ternary molybdate based ceramics with relative permittivity ranging from 4.1 to 50 and Qf from 1,450 to 108,000 GHz [18,]. Some of the reported molybdate based ULTCC materials are Na_2MoO_4 (ε_r = 4.1, Qf = 35,000 GHz, τ_f = -76 ppm/^oC) [19], Li_2MoO_4 (ε_r = 5.5, Qf = 46,000 GHz, τ_f = -160 ppm/^oC) [20], $K_2Mo_4O_{13}$ (ε_r = 6.8, Qf = 39,800 GHz, τ_f = -67 ppm/^oC) [21], $Sm_2Mo_4O_{15}$ (ε_r = 10.7, Qf = 63,500 GHz, τ_f = -50 ppm/^oC) [22], Te_2MoO_7 (ε_r = 13.6, Qf = 46,900 GHz, τ_f = -36 ppm/^oC) [23], Pb_2MoO_5 (ε_r = 19.1, Qf = 21,800 GHz, τ_f = -215 ppm/^oC) [24] and $PbMoO_4$ (ε_r = 26.7, Qf = 42,800 GHz, τ_f = 6 ppm/^oC) [25]. However, there are only a few reports of binary ceramics with low sintering temperatures and low dielectric loss at microwave frequency ranges. According to the ULTCC review, there are only two binary ceramic materials (TeO_2 and Bi_2O_3) reported with firing temperature less than 700 ^oC. The TeO_2 ceramic is reported to have a low sintering temperature of 640 ^oC/15h with ε_r of 19.3, Qf of 30,000 GHz and τ_f of -119 ppm/^oC [18]. Similarly, Bi_2O_3 ceramic was sintered at 680 ^oC with ε_r of 33.5, Qf of 18,700 GHz and τ_f of -235 ppm/^oC [18].

Recently, Vidya *et. al*., in 2015 reported that MoO_3 nanorod ceramics prepared by wet chemical synthesis are suitable for Low-Temperature Co-fired Ceramic (LTCC) and optical applications [26] with a relative permittivity of 8.01 and dielectric loss tangent of 0.02 at 5 MHz after sintering at 700

^{o}C. However, the microwave dielectric properties of MoO_3 ceramics have not yet been reported. In this present paper the structural stability of sintered α-MoO_3 ceramics along with their microwave dielectric properties are studied. The paper also demonstrates the exact correlation between the Qf and Full Width Half Maximum (FWHM) value of the Raman spectrum for samples sintered at various temperatures.

Experimental

MoO_3 bulk samples were prepared by simple solid state sintering and uniaxial pressing from high purity reagent grade MoO_3 (> 99 %, Alfa Aesar). The powder was sieved to an average particle size of 45 μm and, for microwave measurements, was pressed into circular disks (diameter 10 mm and thickness 5 mm) with a uniaxial pressure using 50 MPa. Green samples were sintered in the temperature range of 550-700 ^{o}C. The crystal structure of the specimens was analyzed by X-ray diffractometer (D8, Bruker, Billerica, MA) using Cu Kα radiation. A Thermo Fisher Scientific, ESCALAB 250 Xi using the MgKα X-ray source was used for XPS analysis. Reference energies of Au $4f_{5/2}$ (83.9±0.1 eV) and Cu $2p_{3/2}$ (932.7±0.1 eV) were used for calibrating the spectrometer. The take-off angle (the angle between the surface and the analyzer) was kept at 90^{o} for the measurement. A binding energy of 285.0 eV was assigned to the C 1s peak corresponding to the surface contamination and was used as an internal reference for the correction of charging effects. The energy resolution of the XPS is 0.45 eV. Thermogravimetric (TG) and differential scanning calorimetric (DSC) analysis were carried out using TGA/DTA (NETZSCH, STA 499 F3 Jupiter, Germany) at a heating rate of 2 ^{o}C/min in air. The microstructure analysis of the MoO_3 was performed using scanning electron microscopy (FESEM, ZEISS Ultra Plus, Germany). The optical Raman spectra of the ceramic were measured with signals excited by a 488 nm Ar^{+} laser using a spectrometer (LabRam HR800, Horiba Jobin-Yvon, Villeneuve-d'Arcy, France). The bulk densities of the sintered samples were measured by

the Archimedes method. Relative permittivity, quality factor and temperature coefficient of resonant frequency were measured using Hakki Coleman and cavity methods connected to a vector network analyzer (10 MHz-20 GHz, ROHDE& SCHWARZ, ZVB20, Germany) and temperature chamber (SU-261, ESPEC CORP., Japan) in the temperature range of 25-85 ^{o}C. The temperature variation of relative permittivity and dielectric loss were measured using the Split Post Dielectric Resonator method operated at 9.97 GHz. The total uncertainty of real permittivity did not exceed 0.5% and it was possible to resolve dielectric loss tangents to approximately $5x10^{-5}$ with the SPDR technique [27]. The coefficient of thermal expansion (CTE) was investigated in the temperature range of 25-500°C with cylindrical samples of dimensions 8 mm × 15 mm using a dilatometer (NETZSCH, DIL 402 PC/4, Germany). The dilatometer measurement was performed at a heating rate of 5 ^{o}C/min. The temperature coefficient of resonant frequency (τ_f) was calculated using Equation 1 given below [28]. While f_{-40}, f_{80} are initial and final resonant frequency similarly, T_{-40}, T_{80} represents the initial and final measured temperatures.

$$\tau_f = \frac{f_{80} - f_{-40}}{f_{-40} * (T_{80} - T_{-40})} \, 10^{-6} \quad \text{ppm/}^{o}\text{C} \qquad (1)$$

Porosity corrected relative permittivity was calculated using the modified Bruggeman correction for the two-phase system (solid and air) [28] and is shown in Equation 2, where *P* represents the porosity of the dielectric sample, air permittivity is taken as 1 to simplify the equation, ε_{rc} is the porosity corrected relative permittivity, and ε_{rm} is the measured permittivity of the dielectric sample. This equation is more valid for the higher values of porosity [28].

$$\varepsilon_{rc} = \frac{\varepsilon_{rm}(3P - 1 - 2\varepsilon_{rm})}{3\varepsilon_{rm}P - 1 - 2\varepsilon_{rm}} \qquad (2)$$

The temperature coefficient of relative permittivity (τ_ε) of the sample can be calculated using the equation [28].

$$\tau_\varepsilon = -2(\tau_f + \alpha_L) \quad \text{ppm/}^{o}\text{C} \qquad (3)$$

Where, τ_f is temperature coefficient of resonant frequency from cavity method and α_L is the linear coefficient of thermal expansion from dilatometer.

Result and Discussions

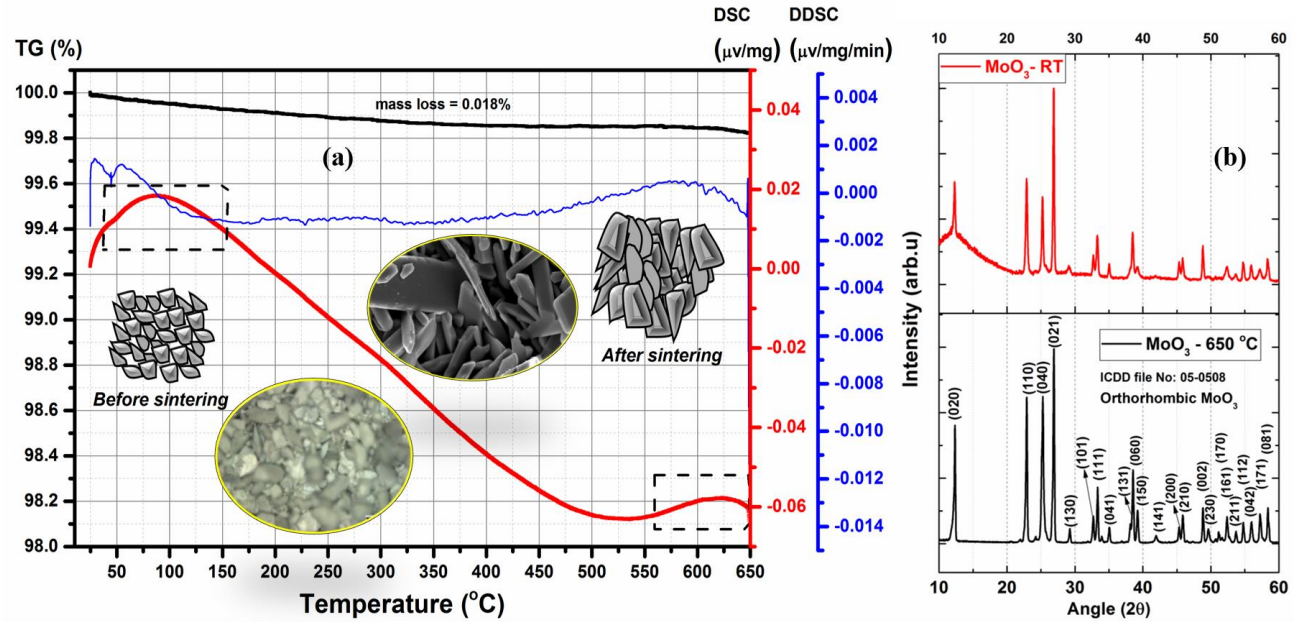

Figure 1. (a). TG, DSC and DDSC curve of MoO_3 ceramic (inset figures show schematically the grain growth before and after sintering with supporting optical and SEM pictures) and (b) X-ray diffraction pattern of MoO_3 powder at room temperature and after sintering at 650 °C.

Figure 1 (a) depicts the TG, DSC, and DDSC of the MoO_3 ceramic sample from room temperature to 650 °C. From the TGA curve, the total mass loss of MoO_3 ceramic was measured to be 0.018 %. The DSC and DDSC curves indicate that the sintering started at above 550 °C. The appearance of grain morphology before and after sintering is shown as optical and SEM images in the insets of Figure 1(a). Figure 1(b) depicts the X-ray diffraction pattern of MoO_3 powder at room temperature (RT) and MoO_3 after sintered at 650 °C indicating that they belonged to the stable phase. All the peaks are indexed based on the stable orthorhombic phase and the corresponding ICDD card no: 05-0508. It is reported that higher intensities of (0 k 0) planes with k = 2, 4 and 6 reveal highly anisotropic grain growth of the oxides [29-31]. The MoO_3 morphology during sintering has previously been well documented by various researchers and is also evident from the (0 k 0) planes present in the

X-ray diffraction [14-17]. In MoO_3 ceramics, highly distorted MoO_6 octahedra, which are interconnected with the edges of the (001) plane and interlinked with the corner sharing (100) plane, lead to a double layer flake-like planar structure. This anisotropic grain growth in the flake-shaped MoO_3 is common with stable α-MoO_3 [32-34]. In the present case the XRD of the MoO_3 sintered at 650 ^oC had intense peaks for (0 k 0) planes such as (0 2 0), (0 4 0) and (0 6 0).

The oxidation behavior and chemical homogeneity of the MoO_3 ceramic were analyzed by the XPS technique. The MoO_3 ceramic sintered at 650 ^oC was used to analyze the spectrum within the surface layer of about 50 Å. The survey spectrum of the MoO_3 is shown in Figure 2 (a). Besides the expected Mo 3d, O 1s peaks**,** a low intense C 1s peak was also observed and is presented in the inset. The C 1s peak did not affect the interpretation of the present results and, in fact, was used for binding energy calibration by setting its binding energy at 284.8 eV for sample charging correction [35, 36]. All the un-indexed peaks in the survey spectrum represent the other characteristic peaks and Auger peaks of Mo and O in the MoO_3 ceramic.

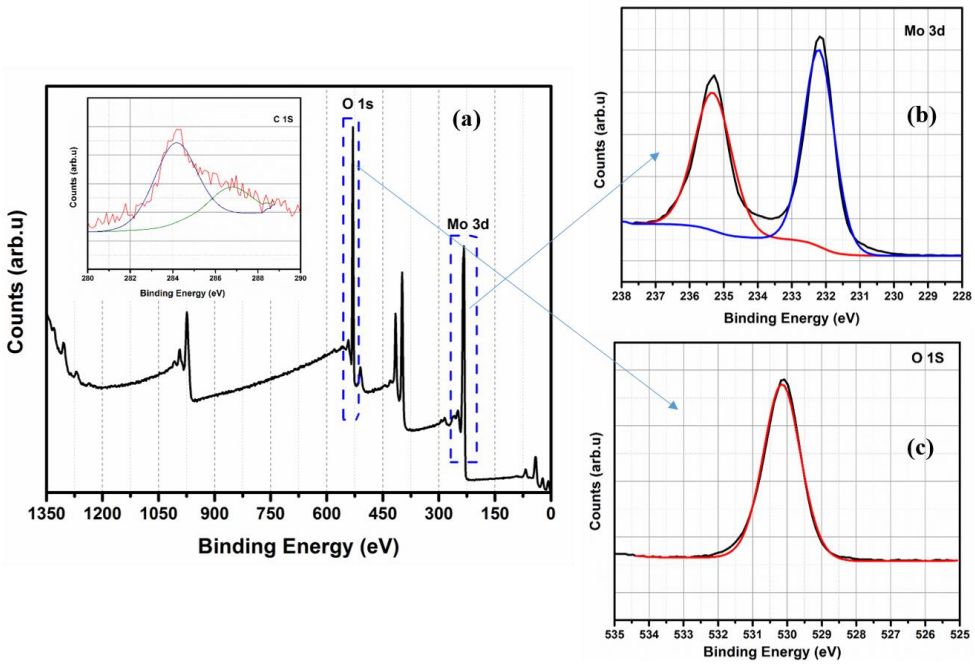

Figure 2 XPS analysis of MoO_3 after sintering at 650 ^oC with (a) survey spectrum and inset figure high resolution carbon 1s peak, (b) fitted high resolution spectrum of Mo 3d and (c) fitted high resolution spectrum of O 1s.

Figure 2 (b) shows the high-resolution spectrum of Mo 3d with spin-orbital splitting $3d_{5/2}$ and $3d_{3/2}$ having an orbital split of about 3.11 eV at a binding energy of 232.21 eV and 235.32 eV, respectively. The Mo 3d fitted binding energies have FWHM of 1.07 and 1.30 eV with atomic wt. % of 3.99 and 3.41 respectively. The Mo 3d scan suggests that Mo in MoO_3 ceramic sintered at 650 ^oC belongs to the 6^+ oxidation state [36]. It confirms that the MoO_3 sintered at 650 ^oC was stable. Core-level spectra of O 1s and its curve fitting for MoO_3 ceramic are shown in Figure 2 (c). This O 1s photoelectron peak provides information on the oxide ion in the sintered MoO_3 ceramics with Mo-O chemical bonding. A well-resolved peak at 530.15 eV fitted with atomic wt. % of 22.87 relates to the bridging oxygen atoms present in the MoO_3 ceramic. The peaks associated with Mo 3d as well as O 1s show good agreement with reported values [37, 38]. The XPS results reveals, especially for Mo was stable at 6^+ oxidation state when it undergoes sintering at 650 ^oC, which confirm the stability of the MoO_3 after sintering process.

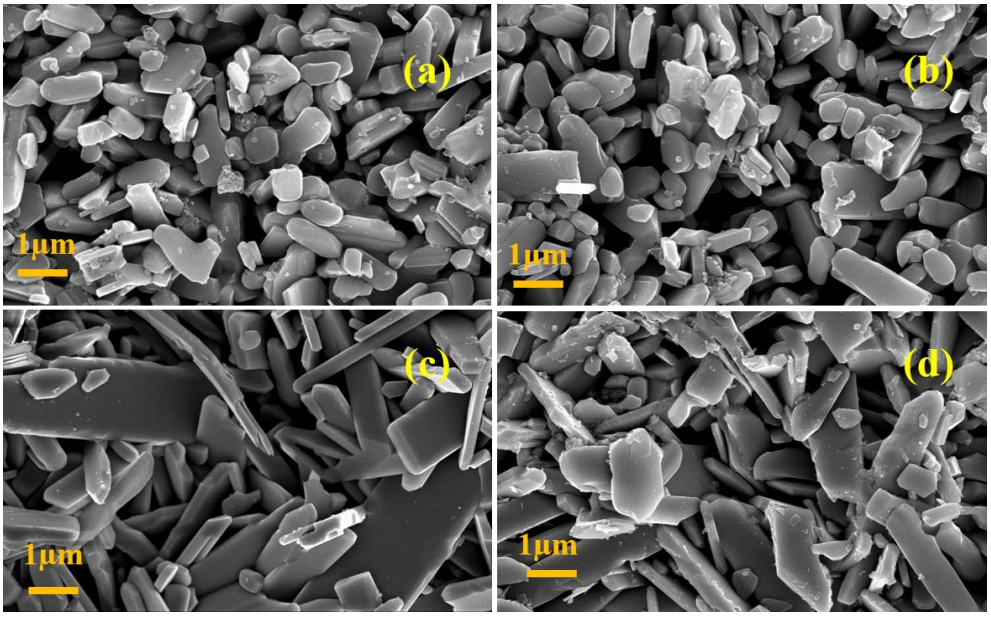

Figure 3 Microstructure of MoO_3 ceramic after sintering at (a) 550 ^oC, (b) 600 ^oC, (c) 650 ^oC and (d) 700 ^oC.

Figure 3 (a) (b) (c) & (d) shows the microstructure of MoO_3 sintered at 550, 600, 650 and 700 ^oC. The abnormal grain growth during sintering at 550-700 ^oC is clear from the SEM images. This

abnormal grain growth restricted the densification for bulk MoO_3 samples to some extent. However, the sample sintered at 650 ^oC (Figure 3 (c)), with fine, and long grains showed the highest densification of 88 %. On the other hand, the grains were smaller and more loosely packed after sintering at 550 and 600 ^oC. The sample sintered at 700 ^oC started to deform slowly due to the melting, sublimation and evaporation of MoO_3, hence exhibiting high porosity. It has been reported that above 700 ^oC the MoO_3 vapor pressure is high and MoO_3 slowly starts to evaporate at this temperature [39, 40].

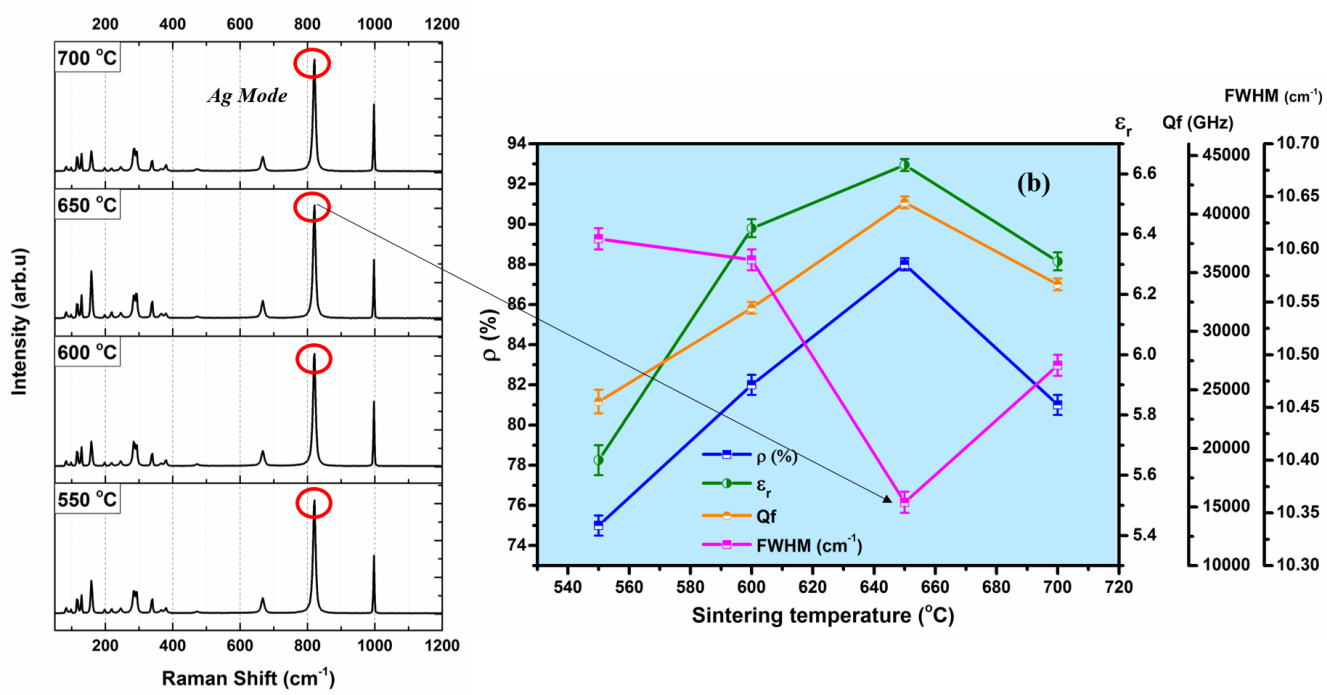

Figure 4 (a) Raman spectrum and (b) densification, relative permittivity, Qf and full width half maximum of MoO_3 sintered at various temperature.

Figure 4 (a) shows the Raman shift of bulk MoO_3 sintered at 550, 600, 650 and 700 ^oC respectively. α-MoO_3 belongs to the space group D_{2h}^{16}, having 16 atoms in the unit cell; four atoms of molybdenum and the remaining atoms are oxygen. According to group theory analysis, 48 vibrational modes are expected. Among these 48 vibrational modes, a total of 24 modes ($8A_g + 8B_{lg} + 4B_{2g} + 4B_{3g}$) are Raman active modes [41-45]. The vibrational modes identified with MoO_3 belong to the stretching, deformation and lattice modes. The Raman peaks at 996 and 821 cm^{-1} are assigned to stretching Ag modes such as asymmetric stretching of Mo=O and doubly coordinated Mo-O-Mo (the corner shared

oxygen present in the MoO_6 octahedra) stretching modes respectively. The peak present at 666 cm^{-1} belongs to the Bg mode assigned to triply coordinated oxygen stretching in the 3 MoO_6 [46]. These three main peaks are referred to as the fingerprint of stable α-MoO_3 [47-49]. All the peaks and corresponding assigned modes in the Raman spectrum of bulk MoO_3 sintered at 650 ^oC were well matched with previous reports in the literature as shown in Table 1. Among the vibration modes, the stretch mode (A_{1g} with wave number around 821 cm^{-1}) of the oxygen octahedra has the sturdiest polarity as well as the strongest intensity and hence exerts a strong impact on the microwave dielectric properties [41, 50, 51].

Table 1 Raman mode assignments of bulk MoO_3 ceramic sintered at 650 ^oC.

Raman shift (cm^{-1})	**Mode assignments Raman active - ($8A_g + 8B_{lg} + 4B_{2g} + 4B_{3g}$)**	**Reference based on previous reports**
996	$A_g + B_{1g}$	41-49
819	$A_g + B_{1g}$	41-49
666	$B_{2g} + B_{3g}$	41-49
472	$A_g + B_{1g}$	41-49
381	B_{1g}	41-49
366	A_g	41-49
339	$Ag + B_{1g}$	41-49
283	$B_{2g} + B_{3g}$	41-49
246	B_{3g}	41-49
219	A_g	41-49
199	B_{2g}	41-49
160	$A_g + B_{1g}$	41-49
130	B_{3g}	41-49
118	B_{2g}	41-49
96	B_{1g}	41-49
83	A_g	41-49

Figure 4 (b) represents the effect of the sintering temperature on densification, relative permittivity (ε_r), quality factor (Qf) and FWHM of the selected A1g mode (high intensity as compared to other A1g modes in the spectrum). The sintering experiments revealed that the densification increased to a maximum when sintered at 650 ^oC and after that showed a slight decrease, this being in line with the microstructural studies. Also, the relative permittivity and Qf of bulk MoO_3 ceramics increased from 5.6 to 6.6 and from 24,000 to 41,000 GHz at 11.3 GHz, respectively, when the sintering temperature was increased from 550 ^oC to 650 ^oC. At the higher temperature of 700 ^oC, the

densification, relative permittivity and Qf of the sample degraded. The porosity corrected relative permittivity of this ceramic was found to be 8 using equation 2 with a theoretical model for high porosity samples by the modified Bruggeman method [28].

The effect of sintering on the double co-ordinated Mo-O-Mo ordering of the ceramic was evident from analysis of the FWHM of the active mode in the Raman spectra. This Raman line exhibited no shift while the FWHM of bulk MoO_3 ceramics varied with sintering temperature. From Figure 4 (b) it is clear that the FWHM decreased with increase in sintering temperature up to 650 ^oC and a further increase in sintering temperature resulted in an increase in FWHM. On the other hand, the Qf value followed the opposite trend (24,000 GHz to 41,000 GHz), and increased linearly with the decrease in FWHM, which is evident from Figure 4 (b). The bulk MoO_3 ceramics sintered at 650 ^oC exhibited a minimum FWHM of the A_{1g} mode which indicated a high degree of ordering and low phonon damping which in turn leads to the higher value of Qf [52]. The decrease of FWHM denotes the weakening of the coherence and damping behavior of the A_{1g} stretching vibration and hence results in the reduction of anharmonic vibrations which in turn relates to low dielectric loss. It eventually leads to the increase in the intrinsic Qf value inversely [53-55]. However, it is noted that bulk MoO_3 ceramics showed a good quality factor even at its relatively low densification of 88 % when sintered at 650 ^oC.

Figure 5 (a) shows the temperature (-40 – 85 ^oC) variation of Qf, and the resonant frequency of bulk MoO_3 ceramics sintered at 650 ^oC. It is noted that the highest Qf of 63,000 GHz was observed when the sample was at the measurement temperature of -40 ^oC and it gradually decreased on heating the sample to 85 ^oC. This is due to the lower phonon vibrations at sub-zero temperature. The resonant frequency also showed a similar trend. The bulk MoO_3 ceramics sample sintered at 650 ^oC showed a temperature coefficient of resonant frequency (τ_f) of -25 ppm/^oC in the temperature range of -40 to 85 ^oC. The sintered MoO_3 sample show linear coefficient of thermal expansion (CTE) of ± 4 ppm/^oC measured in the temperature range of 25 to 500 ^oC. While, the CTE in the measured temperature range

of 25 to 100 ^{o}C is about -2.7 ppm/^{o}C. Based on the τ_f and CTE value, the calculated τ_ε value is about 55 ppm/^{o}C using the equation 3. The calculated τ_ε is positive and 2 time higher than the τ_f and CTE of sintered MoO_3. Figure 5 (b) shows the temperature variation of relative permittivity and dielectric loss of bulk MoO_3 ceramics sintered at 650 ^{o}C and measured using the SPDR technique at 9.97 GHz. It is evident from Figure 5 (b) that relative permittivity and dielectric loss slightly increased with temperature. The sintered MoO_3 substrate shows variation in permittivity upon heating (25 to 85 ^{o}C) is about 0.6 %. However, the observed microwave dielectric properties of MoO_3 will be of great interest for many applications.

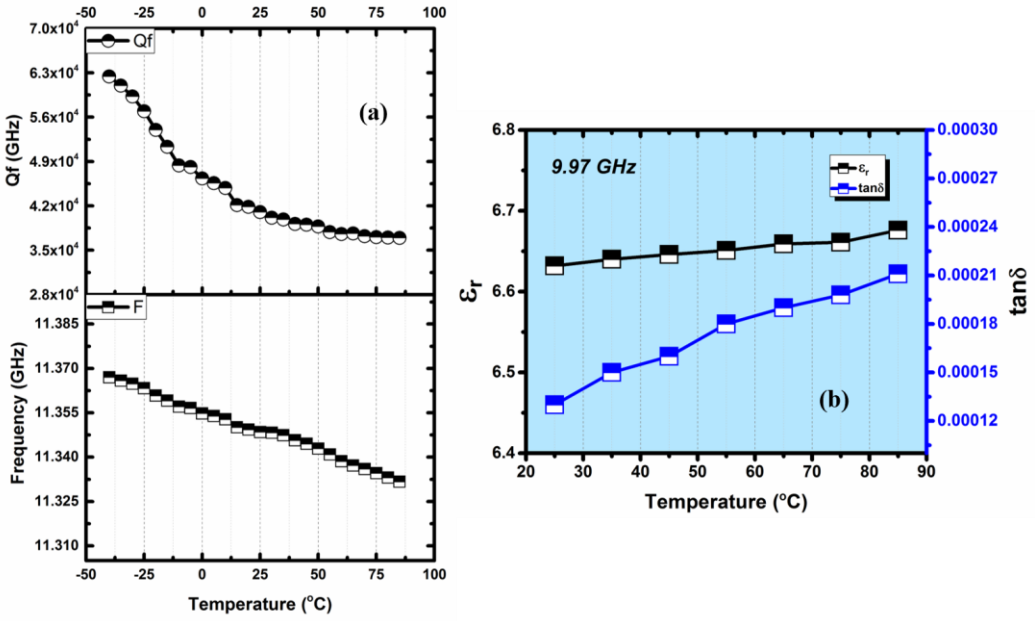

Figure 5 (a) Temperature variation of Qf and resonant frequency and (b) temperature variation of relative permittivity and dielectric loss of bulk MoO_3 ceramic sintered at 650 ^{o}C.

Table 2 shows the comparison of sintering temperature and microwave dielectric properties of low sintering binary ceramics with that of present work. It has been noted that, even with 88 % densification MoO_3 possess moderately high Qf of 41000 GHz and low temperature coefficient of resonant frequency of -25 ppm/^{o}C in comparison with other binary oxide reported. However, it should be noted that most of the molybdates have a strong reaction with Ag and Al, which limits their usage with the commonly used Ag and Al electrodes in LTCC/ULTCC applications [see supporting

information Figure S1]. It has been reported that Ag_2MoO_4 and $Al_2(MoO_4)_3$ are the major intermediate compounds when MoO_3 undergoes reaction with Ag and Al [56]. Still, the low temperature ($\leq 200\ ^oC$) commercial electrode DuPont 8453 may be used as post firing applications for the present binary MoO_3 [57]. In addition to that, most of the reported molybdates [19-25] are water-soluble like reported H_3BO_3/B_2O_3 microwave ceramics [58]. It has been reported that the binary MoO_3 water solubility is 0.490 g/100 mL (28 °C) in comparison with other ternary molybdates reported [59]. The importance of the present work is explore the excellent dielectric properties of the binary MoO_3 ceramics. The reported results will be a suitable reference for the potential growth in the various applications of stable MoO_3 ceramics.

Table 3 Comparison of sintering temperature microwave dielectric properties of low sintering temperature binary ceramics.

Composition	**S.T[&] (°C)**	**ε_r**	**Qf (GHz)**	**τ_f (ppm/°C)**	**Ref.**
TeO_2	640	19.3	30000	-119	18
Bi_2O_3	680	33.5	18700	-235	18
H_3BO_3/B_2O_3	200	2.2	32700	-40	58
MoO_3	650 (±5)	6.6 (±0.02)	41000 (±500)	-25 (±2)	Present work

[&] S.T.: Sintering Temperature

Conclusion

The bulk α-MoO_3 ceramics were prepared by uniaxial pressing and sintering. This was followed by studies of the microstructure, densification, thermal and microwave dielectric properties. The XPS and Raman studies revealed the quality and quantity of the stable α-MoO_3 ceramics developed. The optimized sintering temperature of MoO_3 ceramics obtained was 650 ^{o}C according to the highest densification and microwave dielectric properties. After sintering the measured relative permittivity was 6.6 and the quality factor (Qf) was 41,000 GHz at the resonance frequency of 11.3 GHz. The full-

width half maximum (FWHM) of the A_{1g} Raman mode of the bulk α-MoO_3 ceramics at different sintering temperatures correlated well with the Qf values. The sintered samples showed a temperature coefficient of the resonant frequency of -25 ppm/^oC in the temperature range of -40 to 85 ^oC. The sintered α-MoO_3 ceramics showed a very low coefficient of thermal expansion of ±4 ppm/^oC measured in the temperature range of 25-500 ^oC. According to our best knowledge, this is the first time that the microwave dielectric properties of stable α-MoO_3 ceramic have been reported.

Acknowledgements

The authors are thankful to European Research Council Project No: 24001893 for financial support. Also, Mr. Santtu Heinilehto (Application Engineer) for XPS and Mr. Pekka Moilanen for Raman spectroscopy measurements are acknowledged.

References

1. M. Kassem, Investigation of Structural and Textural Properties of Ge_xMoO_3 System, Promising Catalyst for Photocatalytic Applications, *Kinet. Catal.* 2016, **57**,26–31.
2. N. H. H. Phuc, P. T. T. Phuong, V. T. Tai, N. M. Huan, N. P. H. Duy, L. C. Loc, Synthesis of a-MoO_3 Thin Sheets and Their Catalytic Behavior for Selective Oxidation of Methanol to Formaldehyde, *Catal. Lett.*, 2016, **146**, 391–397.
3. R. Verma, R. K. Raman,U. V. Varadaraju, Disodium dimolybdate: a potential high-performance anode material for rechargeable sodium ion battery applications, *J. Solid State Electrochem.,* 2016, **20**, 1501–1505.
4. C.V. Subba Reddy, Z. R. Deng, Q.Y. Zhu, Y. Dai, J. Zhou, W. Chen, S.-I. Mho, Characterization of MoO_3 nanobelt cathode for Li-battery applications, *Appl. Phys. A*, 2007, **89**, 995–999.

5. H. C. Xuan, Y. Q. Zhang, Y. K. Xu, H. Li, P. D. Han, D. H. Wang,Y. W. Du, A facile route to large-scale synthesis MoO_2 and MoO_3 as electrode materials for high-performance supercapacitors, *Phys. Status Solidi A,* 2016, 1–6. DOI 10.1002/pssa.201533069.
6. L. Zheng, Y. Xu, D. Jin,Y. Xie, Novel Metastable Hexagonal MoO_3 Nanobelts: Synthesis, Photochromic, and Electrochromic Properties, *Chem. Mater.,* 2009, **21**, 5681–5690.
7. K. A. Gesheva, T. Ivanova, A Low-Temperature Atmospheric Pressure CVD Process for Growing Thin Films of MoO_3 and MoO_3-WO_3 for Electrochromic Device Applications, *Chem. Vap. Deposition,* 2006, **12**, 231–238.
8. K. Galatsis, Y. Li,W. Wlodarski, C. Cantalini, M. Passacantando S. Santucci, MoO_3, WO_3 Single and Binary Oxide Prepared by Sol-Gel Method for Gas Sensing Applications, *J. Sol-Gel Sci. Techn.,* 2003, **26**, 1097–1101.
9. D. Lee, D. Seong, I. Jo, F. Xiang, R. Dong, S. Oh, H. Hwang, Resistance switching of copper doped MoO_x films for nonvolatile memory applications, *Appl. Phys. Lett.,* 2007, **90**, 122104-1-3-.
10. M. T. Greiner, Z.-H. Lu, Thin-film metal oxides in organic semiconductor devices: their electronic structures, work functions and interfaces. *NPG Asia Mater.,* 2013, **5**, e55-1-16. doi:10.1038/am.2013.29.
11. Z. Wang, R. Freer, Low firing temperature zinc molybdate ceramics for dielectric and insulation applications, J.Eur.Ceram.Soc., 2015, **35**, 3033–3042.
12. K. Majhi , L. Bertoluzzi , K. J. Rietwyk , A. Ginsburg , D. A. Keller, P. L.-Varo , A. Y. Anderson , J. Bisquert ,A. Zaban, Combinatorial Investigation and Modelling of MoO_3 Hole-Selective Contact in TiO_2 |Co_3O_4 |MoO_3 All-Oxide Solar Cells, *Adv. Mater. Interfaces*, 2016, **3**, 1500405-1-7, DOI: 10.1002/admi.201500405.

13. V. V. Atuchin T. A.Gavrilova, T. I. Grigorieva, N. V. Kuratieva , K. A. Okotrub , N. V. Pervukhina , N. V. Surovtsev, Sublimation growth and vibrational microspectrometry of a-MoO_3 single crystals, *J. Cryst. Growth*, 2011, **318,** 987–990.
14. B. Xu, Y. Li, G. Wang, D. Zhao, K. Pan, B. Jianq, W. Zhou, H. Fu, In situ synthesis and high adsorption performance of MoO_2/Mo_4O_{11} and MoO_2/MoS_2 composite nanorods by reduction of MoO_3, Dalton Trans., 2015, 44, 6224-6228.
15. H.-J. Lunk, H. Hartl, M. A. Hartl, M. J. G. Fait, I. G. Shenderovich, M. Feist, T. A. Frisk, L. L. Daemen, D. Mauder, R. Eckelt, A. A. Gurinov, Hexagonal molybdenum trioxide—known for 100 years and still afountof new discoveries, *Inorg.Chem.* 2010, **49** ,9400–9408.
16. V. Kumar, A. Sumboja, J. Wang, V. Bhavanasi, V. C. Nguyen, P. S. Lee, Topotactic Phase Transformation of Hexagonal MoO_3 to Layered MoO_3‑II and Its Two-Dimensional (2D) Nanosheets, *Chem. Mater*,. 2014, **26**, 5533−5539.
17. Y. Jin, N. Li, H. Liu, X. Hua, Q. Zhang, M. Chen, F. Teng, Highly efficent degradation of dye pollutants by Ce-doped MoO_3 catalyst at room temperature, Dalton Trans., 2014, 43, 12860-12870.
18. M. T. Sebastian, H. Wang, H. Jantunen, Low temperature co-fired ceramics with ultra-low sintering temperature: A review, *Curr. Opin. in Solid State Mater. Sci.*, 2016, **20**, 151-170.
19. G.-Q. Zhang, H. Wang, J. Guo, L. He, D.-D. Wei, Q.-B. Yuan, Ultra low sintering temperature microwave dielectric ceramics based on Na_2O–MoO_3 binary system, *J. Am. Ceram. Soc.*, 2015, **98**, 528–533.
20. D. Zhou, C. A. Randall, H. Wang, L.-X. Pang, X. Yao, Microwave dielectric ceramics in Li_2O–Bi_2O_3–MoO_3 system with ultra-low sintering temperatures, *J. Am. Ceram. Soc.*, 2010, **93**, 1096–1100.

21. K. Ju, H. Yu, L. Ye, G. Xu, Ultra low temperature sintering and dielectric properties of SiO_2 filled glass composites, *J. Am. Ceram. Soc.*, 2013, **96**, 3563–3568.

22. A. Surjith, E. K. Suresh, S. Freddy, R. Ratheesh, Microwave dielectric properties of low temperature sinterable $RE_2Mo_4O_{15}$ (RE = Nd, Sm) ceramics for LTCC applications, *J. Mater. Sci. Mater. Electron.*, 2013, **24**, 1818–1822.

23. S.-F.- Wang, Y.-R. Wang, Y.-F. Hsu, H.-C. Lu, J.S. Tsai, Ultra low fire $Te_2(Mo_{1\_x}W_x)O_7$ ceramics: microstructure and microwave dielectric properties, J. Am. Ceram. Soc. **93**, 4071–4074.

24. H. Xie, H. Xi, C. Chen, X. Wang, Di Zhou. Microwave dielectric properties of Pb_2MoO_5 ceramics with ultralow sintering temperature, *J. Eur. Ceram. Soc.*, 2014, **34**, 4089-4093.

25. H.- H. Xi, D. Zhou, B. He, H. –D. Xie, Microwave dielectric properties of scheelite structured $PbMoO_4$ ceramic with ultralow sintering temperature, *J. Amer. Ceram. Soc.*, 2014, **97**, 1375- 1378.

26. S. Vidya, S. Solomon, J. K. Thomas, Sythesis and characterization of MoO_3 and WO_3 nanorods for low temperature co-fired ceramic and optical applications, *J. Mater. Sci. Mater Electron*, 2015, **26**, 3243-3255.

27. J. Krupka, A. P. Gregory, O. C. Rochard, R. N. Clarke, B. Riddle, J. J. B. *J. Eur. Ceram. Soc.*, 2001, **10**, 2673–2676.

28. M. T. Sebastian, R. Ubic, H. Jantunen, Low-loss dielectric ceramic materials and their properties, *Int. Mater. Rev.*, 2016, **60**, 392-412.

29. S. Wang, Y. Zhang, X. Ma, W. Wang, X. Li, Z. Zhang, Y. Qian, *Solid State Commun.*, 2005, **136**, 283-287.L. Cheng, M. Shao, X. Wang, H. Hu, Single-Crystalline Molybdenum Trioxide Nanoribbons: Photocatalytic, Photoconductive, and Electrochemical Properties, *Chem. Eur. J.* 2009, **15**, 2310-2316.

30. Ch. V. S. Reddy, E. H. Walker Jr., C. Wen, S. Mho, Hydrothermal synthesis of MoO_3 nanobelts utilizing poly(ethylene glycol), *J. Power Sources*, 2008, **183**, 330-333.

31. O. Yayapoa, A. Phuruangrat, T. Thongtem, S. Thongtem, Synthesis, Characterization and Electrochemical Properties of α-MoO_3 Nanobelts for Li-Ion Batteries, *Russ. J. Phys. Chem. A*, 2016, **90**, 1224-1230.
32. W. Li, F. Cheng, Z. Tao, J. Chen, Vapor-Transportation Preparation and Reversible Lithium Intercalation /Deintercalation of r-MoO_3 Microrods, *J. Phys. Chem. B*, 2006, **110**, 119-124.
33. R. Coquet, D. J. Willock, The (010) surface of α-MoO3, a DFT + U study, *J. Phys. Chem. Chem. Phys.*, 2005, **7**, 3819-3828.
34. N. Floquet, O. Bertrand, J. J. Heizmann, Structural and morphological studies of the growth of MoO_3 scales during high-temperature oxidation of molybdenum, *Oxid. Met.*, 1992, **37**, 253-280.
35. A. M. M. Miguel, Z. Maider, C. M. Elizabeth, E. B.;Aitor, R. Teo´filo, C. C. Montse, Composition and Evolution of the Solid-Electrolyte Interphase in $Na_2Ti_3O_7$ Electrodes for Na-ion Batteries: XPS and Auger Parameter Analysis, *ACS Appl. Mater. Interfaces*, 2015, **7**, 7801-7808.
36. http://srdata.nist.gov/xps/main_search_menu.aspx (Date searched 16.11.2016).
37. T. Brezesinski, J. Wang, S. H. Tolbert, B. Dunn, Ordered Mesoporous α-MoO_3 with Iso-oriented Nanocrystalline Walls for Thin-Film Pseudo capacitors, *Nat. Mater.*, 2010, **9**, 146-151.
38. R. S. Iordanova, M. K. Milanova,K. L. Kostov, Glass formation in the MoO_3-CuO System, *Phy. Chem. Glasses: Eur. J. Glass Sci. Technol. B*, 2006, **47**, 631-637.
39. E. A. Gulbransen, K. F. Andrews, F. A. Brassart, Vapor Pressure of Molybdenum Trioxide, J. Electrochem. Soc., **1963**, 110, 242-243.
40. M. S. Chandrasekharaiah, in: J. L. Margrave (Ed.), The Characterization of High Temperature Vapors, Wiley, New York, **1967**, p.497.

41. N. Joseph, J. Varghese, T. Siponkoski, M. Teirikangas, M. T. Sebastian, H. Jantunen, Glass-Free $CuMoO_4$ Ceramic with Excellent Dielectric and Thermal Properties for Ultralow Temperature Cofired Ceramic Applications, *ACS Sustainable Chem. Eng.*, **2016**, 4, 5632–5639.

42. G. Mestl, P. Ruiz, B. Delmon, H. Knözinger, Oxygen-Exchange Properties of MoO_3: An in Situ Raman Spectroscopy Study, *J. Phys. Chem.*, 1994, **98**, 11269-11275.

43. L. Seguin, M. Figlarz, R. Cavagnat, J. C. Lasskgues, Infrared and Raman spectra of MoO_3 molybdenum trioxides and MoO_3. xH_2O molybdenum trioxide hydrates, *Spectrochem. Acta Part A*, 1995, **51**, 1323-1344

44. D. Liu, W. W. Lei, J. Hao, D. D. Liu, B. B. Liu, X. Wang, X. H. Chen, Q. L. Cui, G. T. Zou, J. Liu, S. Jiang, High-pressure Raman scattering and x-ray diffraction of phase transitions in MoO_3, *J. Appl. Phys.*, 2009, **105**, 023513-1.

45. J. V. Silveria, J. A. Batista, G. D. Saraiva, J. M. Filho, A. G. S. Filho, S. Hu, X. Wang, Temperature dependent behavior of single walled MoO_3 nanotubes: A Raman spectroscopy study, *Vib. Spectrosc.* 2010, **54**, 179-183.

46. H. Sinaim, D. J. Ham, J. S. Lee, A. Phuruangrat, S. Thongtem, T. Thongtem, Free-polymer controlling morphology of α-MoO_3 nanobelts by a facile hydrothermal synthesis, their electrochemistry for hydrogen evolution reactions and optical properties, *J. Alloys Compd.* 2012, **516**, 172-178.

47. D. Wang, J. N. Li, Y. Zhou, D. H. Xu, X. Xiong, R. W. Peng, M. Wang, Van der Waals epitaxy of ultra thin α-MoO_3 sheets on mica substrate with single unit cell thickness, *Appl. Phys. Lett.*, 2016, **108**, 053107,http://dx.doi.org/10.1063/1.4941402.

48. D. Liu, W. W. Lei, J. Hao, D. D. Liu,B. B. Liu, X. Wang, X. H. Chen, Q. L. Cui, G. T. Zou, J. Liu, S. Jiang, High-pressure Raman scattering and x-ray diffraction of phase transitions in MoO3, J. *Appl. Phys.*, 2009, **105**, 023513 http://dx.doi.org/10.1063/1.3056049.

49. X. Chen, W. Lei, D. Liu, J. Hao, Q. Cui, G. Zou, Synthesis and Characterization of Hexagonal and Truncated Hexagonal Shaped MoO_3 Nanoplates , *J. Phys. Chem.*, C, 2009, **113**, 21582-21585.

50. S. Phadungdhitidhada, P. Mangkorntong, S. Choopun, N. Mangkorntong, Raman scattering and electrical conductivity of nitrogen implanted MoO_3 whiskers, *Ceram. Int.*, 2008, **34**, 1121-1125.

51. Y. Dai, G. Zhao, H. Liu, First-Principles Study of the Dielectric Properties of $Ba(Zn_{1/3}Nb_{2/3})O_3$ and $Ba(Mg_{1/3}Nb_{2/3})O_3$, *J. Appl. Phys*., 2009, **105**, 034111-1-9.

52. X. Lu, Y. Zheng, Q. Huang, Z. Dong, Structural Dependence of Microwave Dielectric Properties of Spinel-Structured $Li_2ZnTi_3O_8$ Ceramic: Crystal Structure Refinement and Raman Spectroscopy Study, *J. Electron. Mater.*, 2016, **45**, 940-946.

53. C. T. Lee, Y. C. Lin, C. Y. Huang, Cation Ordering and Dielectric Characteristics in Barium Zinc Niobate, *J. Am. Ceram. Soc.*, 2007, **90**,483-489.

54. J. Guo, C. A. Randall, D. Zhou, G. Zhang, C. Zhang, B. Jin, H. Wang, Correlation between vibrational modes and dielectric properties in $(Ca1-3xBi2xx)MoO_4$ ceramics, *J. Eur. Ceram. Soc*., 2015, **35**, 4459-4464.

55. Q. Liao, Y. Wang, F. Jiang, D. Guo, Ultra-Low Fire Glass-Free $Li_3FeMo_3O_{12}$ Microwave Dielectric Ceramics, *J. Am. Ceram. Soc.* 2014**, 97,** 2394-2396.

56. M. T. Fabbro, Camila C. Foggi, L. P. S. Santos, L. Gracia, A. Perrin, C. Perrin, C. E. Vergani, A. L. Machado, J. Andrés, E. Cordoncillo, E. Longo, Synthesis, antifungal evaluation and optical properties of silver molybdate microcrystals in different solvents: a combined experimental and theoretical study, *Dalton Trans.*, 2016, **45,**10736-10743.

57. http://www.dupont.com/content/dam/dupont/products-and-services/electronic-and-electrical-materials/documents/prodlib/8453.pdf (access date 8th August 2017).

58. L.-X. Pang, D. Zhou, W.-B. Li, Z.-X. Yue, High quality microwave dielectric ceramic sintered at extreme-low temperature below 200ºC and co-firing with base metal, *J. Eur. Ceram. Soc*., 2017, **37**, 3073–3077.

59. M.-H. Lo, F.-H. Cheng, W.-C. J. Wei, Preparation of Al_2O_3/Mo nanocomposite powder via chemical route and spray drying, *J. Mater. Res*., 1996, **11**, 2020-2028.

TOC Graph

TOC Synopsis: Raman spectrum, low temperature sintering and high quality factor α-MoO_3 binary ceramics